Nano Energy 53 (2018) 440–448

Contents lists available at ScienceDirect

Nano Energy

journal homepage: www.elsevier.com/locate/nanoen

Full paper

All electrospray printed perovskite solar cells

Yuanyuan Jiang[a,b,c,1], Congcong Wu[b,1], Liurui Li[c], Kai Wang[b], Zui Tao[d], Fan Gao[c], Weifeng Cheng[c], Jiangtao Cheng[c], Xin-Yan Zhao[d], Shashank Priya[b,e,*], Weiwei Deng[a,c,**]

[a] Department of Mechanics and Aerospace Engineering, Southern University of Science and Technology, Shenzhen 518055, China
[b] Center for Energy Harvesting Materials and System (CEHMS), Virginia Tech Blacksburg, VA 24061, United States
[c] Mechanical Engineering Department, Virginia Tech, Blacksburg, VA 24061, United States
[d] SUSTech Academy for Advanced Interdisciplinary Studies, Southern University of Science and Technology, Shenzhen 518055, China
[e] Materials Research Institute, Penn State, University Park, PA 16802, United States

ARTICLE INFO

Keywords:
Perovskite solar cell
Electrospray printing
Scalable manufacturing

ABSTRACT

The power conversion efficiencies of perovskite solar cells (PSCs) have reached 23.3% recently, rivaling those of established photovoltaic technologies. For PSCs to be commercially competitive, one of the important challenges is to overcome the limitations of small area and excessive material waste from spin-coating. Electrospray printing is a scalable and roll-to-roll compatible method with high material utilization rate. Here, we report an all electrospray printing process for PSCs in ambient air below 150 °C. Strategies for successful electrospray printing of PSCs include formulating the precursor inks with solvents of low vapor pressures and judicial choice of droplet flight time, as well as tailoring the wetting property of the substrate to suppress coffee ring effects. Implementation of these strategies leads to pin-hole free, smooth and uniform perovskite layer, hole transport layer and electron transport layer. The power conversion efficiency of the all electrospray printed devices reaches up to 15.0%, which is the highest to date for fully printed PSCs using mainstream printing methods in air without significant material waste.

1. Introduction

Hybrid organic-inorganic lead halide perovskites have emerged as promising photovoltaic materials because of their outstanding optoelectronic characteristics such as the broadband light absorption, high ambipolar mobilities, and long charge-carrier diffusion lengths [1,2]. In addition, lead halide perovskites can be synthesized using low-cost and earth-abundant raw materials through solution-based process at moderate temperatures (below 150 °C), rendering them promising candidates for low-cost thin film photoenergy conversion devices. Within eight years, the power conversion efficiencies (PCEs) of perovskite solar cells (PSCs) have leapfrogged from 3.8% to a certified 23.3% [3–6]. To make PSCs commercially competitive, one of the remaining challenges is to develop a facile and cost-effective scalable printing process. Two categories of scalable methods for fabricating perovskite films have been successfully demonstrated: (i) continuous deposition such as slot-die coating [7,8] and doctor blade coating [9–12]; (ii) dispersed deposition based on overlapping of individual impacting droplets, such as inkjet printing [13] and spray coating [14], which can conformally deposit films on curved surface and are more tolerant to the roughness or non-flatness of substrates. Most spray deposition methods such as air-brush and blow dryer require strong gas flow to atomize, spread, or dry the liquid [14,15]. The strong gas flow may blow away active ingredients in the liquid phase to cause excessive material waste. Electrospray, in contrast, does not require the assistance of gas flow because it uses electric field to generate uniform charged droplets [16]. The Coulombic attraction force between the droplets and the substrate suppress droplet rebound hence material waste is minimized [17]. Because electrospray is also scalable and roll-to-roll compatible, recently there has been growing interest in the application of electrospray deposition for perovskite thin films using one-step or two-step method [18–20]. Kavadiya et al. optimized the two-step fabrication of perovskite film by electrospray and discovered the enhanced device stability with electrosprayed perovskite film over the spin-coated ones and the PCE reaches 12% [20]. In all these prior studies, the PCEs of the PSCs with electrosprayed perovskite layer still lag noticeably behind their spin-coated counterparts. Additionally, only the perovskite layer was fabricated using electrospray in these studies, while the electron

* Corresponding author at: Materials Research Institute, Penn State, University Park, PA 16802, United States.
** Corresponding author at: Department of Mechanics and Aerospace Engineering, Southern University of Science and Technology, Shenzhen 518055, China.
E-mail addresses: spriya@vt.edu (S. Priya), dengww@sustc.edu.cn (W. Deng).
[1] These authors contributed equally.

https://doi.org/10.1016/j.nanoen.2018.08.062
Received 16 July 2018; Received in revised form 19 August 2018; Accepted 27 August 2018
Available online 07 September 2018

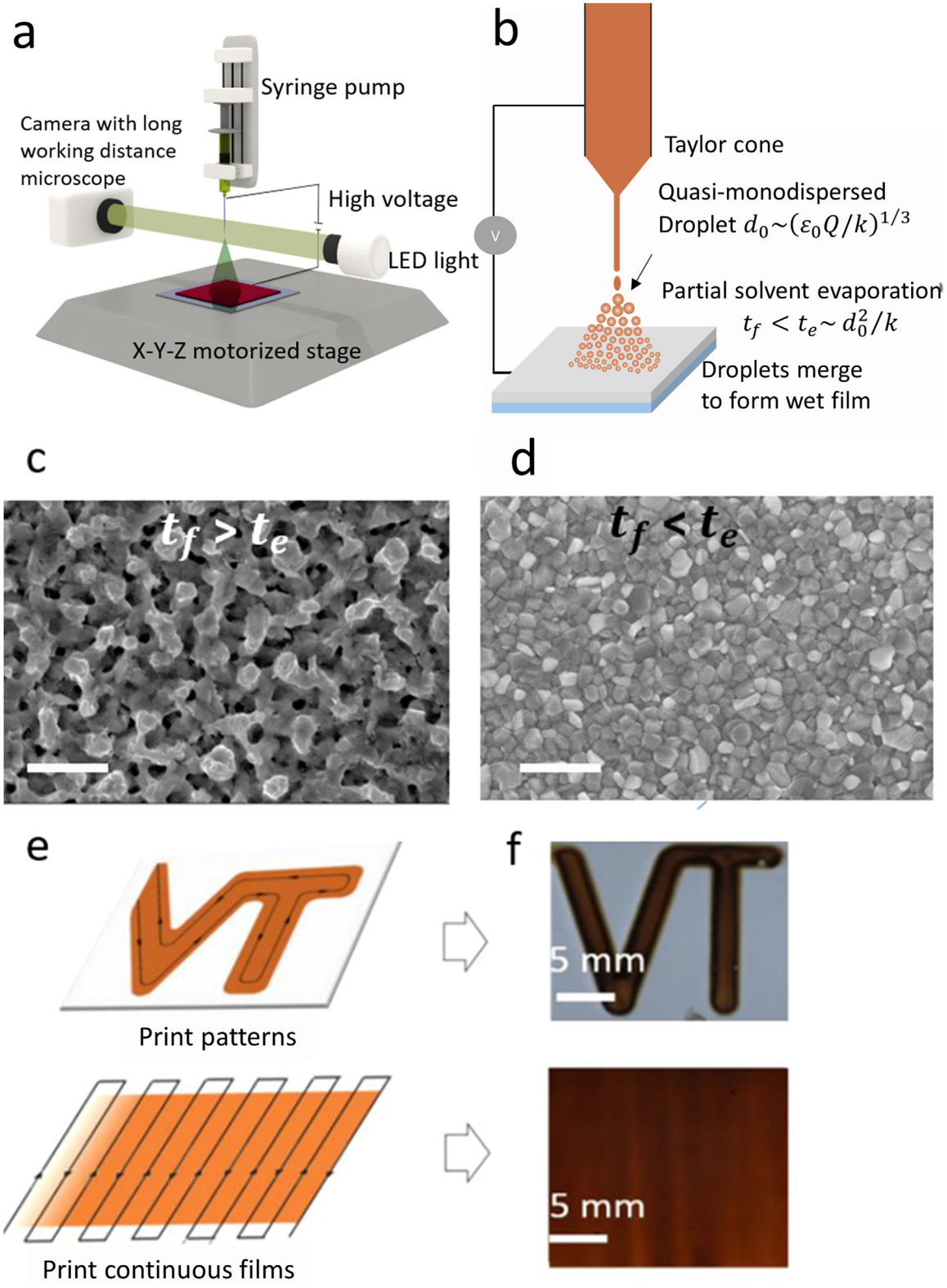

Fig. 1. (a) Scheme of electrospray printing system. (b) Diagram of electrospray printing process. (c) Top-view SEM images electrospray printed film when $t_f > t_e$ and (d) when $t_f < t_e$; the scale bar is 1 μm. (e) Scheme for path motion of electrospray nozzle relative to substrate to print VT-shaped patterns and continuous film. f) Photos of electrospray printed VT-shaped pattern of perovskite, and a square perovskite film with area of 20 mm × 20 mm.

transport layer (ETL) and hole transport layer (HTL) were still prepared by conventional spin-coating. It is highly desirable to apply one type of printing process to fabricate all functional layers.

Here we report a universal electrospray process to print the perovskite layer, HTL and ETL of the PSCs in ambient air environment at modest temperatures. Specifically, the precursor ink formulation and printing parameters were judicially chosen to make the time of flight shorter than the evaporation time of the droplet, thereby promoting the formation of continuous wet precursor films that lead to high-quality dry functional films. Smooth and pin-hole free 300–500 nm perovskite

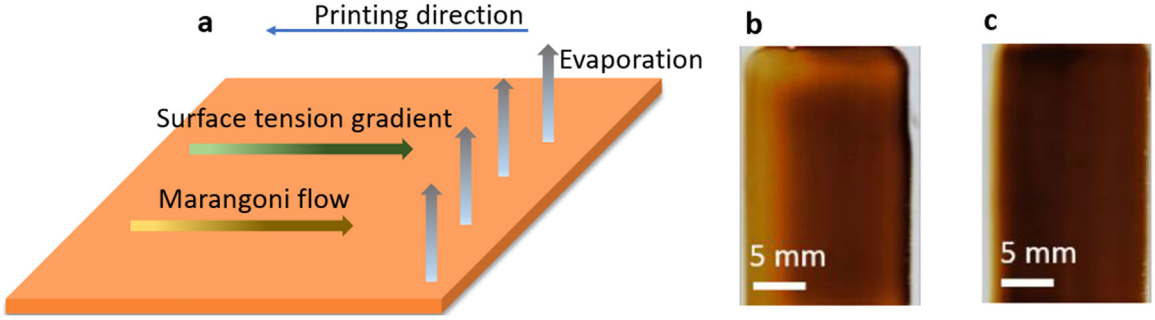

Fig. 2. (a) Schematic illustration for the directional microscale solution flow. (b) Optical image of perovskite films obtained from nearly 0° contact angle and (c) 18° contact angle.

layer, 90 nm TiO_2-based ETL and 140 nm Spiro-OMeTAD based HTL were successfully electrospray printed in ambient air below 150 °C. The all electrospray printed devices exhibited a PCE up to 15.0%.

2. Results and discussion

2.1. Principle for printing wet precursor films with electrospray

A typical electrospray system (Fig. 1a) can be implemented by feeding a liquid with sufficient electrical conductivity through a small capillary that is charged to a few kV relative to a nearby ground electrode. The liquid encompasses a conical shape (termed Taylor-cone [21]) with an electrified fine jet issuing from the cone. The jet undergoes the Rayleigh-Plateau instability [16] and breaks up into ultrafine and quasi-monodispersed droplets.

For printing methods based on individual droplets to eventually achieve smooth and dense dry films without pin-holes, it is essential to form continuous wet precursor films. To that end, the droplets should remain fluidic upon impacting the substrate, allowing the droplets to merge with each other and become part of a continuous wet film. Otherwise, the droplet would dry prematurely, and the substrate will only collect nanoparticles, resulting in a rough and porous film with many voids (Fig. 1c). The degree of solvent evaporation from the droplets as they travel toward the substrate is determined by the ratio of time of flight t_f and droplet evaporation time t_e. t_e is approximately proportional to the surface area of the droplet [22] and can be estimated by the d-square law [23]:

$$t_e = \frac{{d_0}^2}{K}, \tag{1}$$

where d_0 is the initial droplet diameter, and K is the solvent evaporation rate. d_0 can be estimated by the scaling law [21]:

$$d_0 = G(\varepsilon)(\varepsilon\varepsilon_0 Q/\kappa)^{1/3}, \tag{2}$$

where G is a constant of order one, ε is the dielectric constant, ε_0 is the vacuum permittivity, Q is the liquid flow rate, and κ is the liquid electrical conductivity. The evaporation rate K for an isolated spherical droplet can be estimated by the established mass transfer models [24,25]:

$$K = 8D_{diff}\frac{\rho_g}{\rho}\frac{P_v}{P_0}\exp\left(\frac{4\sigma v_m}{d_0 RT}\right), \tag{3}$$

where D_{diff} is the mass diffusivity of the vapor molecule to the ambient environment (usually air), ρ_g is the solvent vapor density, ρ is the liquid density, P_v/P_0 is the ratio of vapor pressure of the solvent to ambient pressure, σ is the surface tension, v_m is the molar volume of the liquid, R is the universal gas constant, and T is the temperature. Eq. (3) suggests that the evaporation rate is proportional to solvent vapor pressure.

2.2. Electrospray printing of perovskite layers

At a typical perovskite precursor flow rate of 0.72 μL/min and κ = 4.3 S/m, the estimated initial droplet diameter is ~ 130 nm, which is prone to rapid drying according to Eq. (1). To ensure wet deposition, we used the mixture of γ-Butyrolactone (GBL) and 1-Methyl-2-pyrrolidinone (NMP) as the solvent, both of which have very low vapor pressure (1.5 mm Hg for GBL and 0.29 mm Hg for NMP at 20 °C) to increase t_e to ~ 10^{-4} s. The working distance between the nozzle and the substrate is decreased to 1.2 mm to reduce t_f so that t_f is shorter than or comparable with t_e, as schematically illustrated in Fig. 1b. Different ratios of t_f over t_e will lead to different outcomes of either nanoporous perovskite film ($t_f > t_e$) or dense perovskite film ($t_f < t_e$), as shown in Fig. 1c and d.

The thickness of the dry perovskite film can be controlled by precursor solution concentration and printing parameters, as expressed in Eq. (4):

$$\delta = \frac{Q\phi}{VX_{offset}}, \tag{4}$$

where δ is the film thickness, ϕ is the volume concentration of the precursor, X_{offset} is the distance between two adjacent printing paths and V is the stage moving speed. Hence, the film thickness can be precisely prescribed. Once the printing conditions ensure the formation of wet films, we can choose proper X_{offset} and serpentine path to form continuous films with desired film thickness according to Eq. (4), or directly print pre-programmed pattern, such as “VT” in Fig. 1e and Fig. 1 f.

We also found that appropriate contact angles between the perovskite precursor solution and the substrate are critical to form uniform films. We found that for the as-prepared TiO_2 film surface after annealing at 150 °C for 30 min, the contact angle is nearly 0°, while after the TiO_2 surface is post-processed simply by exposing to the vacuum environment, the contact angle is increased to ~ 18°. The mechanism of this change of contact angle is unknown. Nevertheless, the contact angle profoundly affects the printing outcome. Fig. 2b shows that for small contact angle, the solution can spread on the substrate, leading to an inhomogeneous film, as indicated by the obvious change in shades of brown color (Fig. 2b). When the contact angle is increased to ~ 18°, the variation of color becomes much less, suggesting that the thickness of the film is more uniform (Fig. 2c). This phenomenon can be explained by the Marangoni effect [26] that is induced by the surface tension gradient caused by uneven solvent evaporation as shown in Fig. 2a. Small contact angle corresponds to more uneven evaporation that causes stronger Marangoni flow to convect the liquid from the freshly printed region to the semi-dried edge (Fig. 2b). As the contact angle increases, the Marangoni flow becomes weaker and the film becomes evener (Fig. 2c).

The printed wet perovskite precursor film immediately undergoes vacuum flash drying [27]. There exists a certain film thickness range for

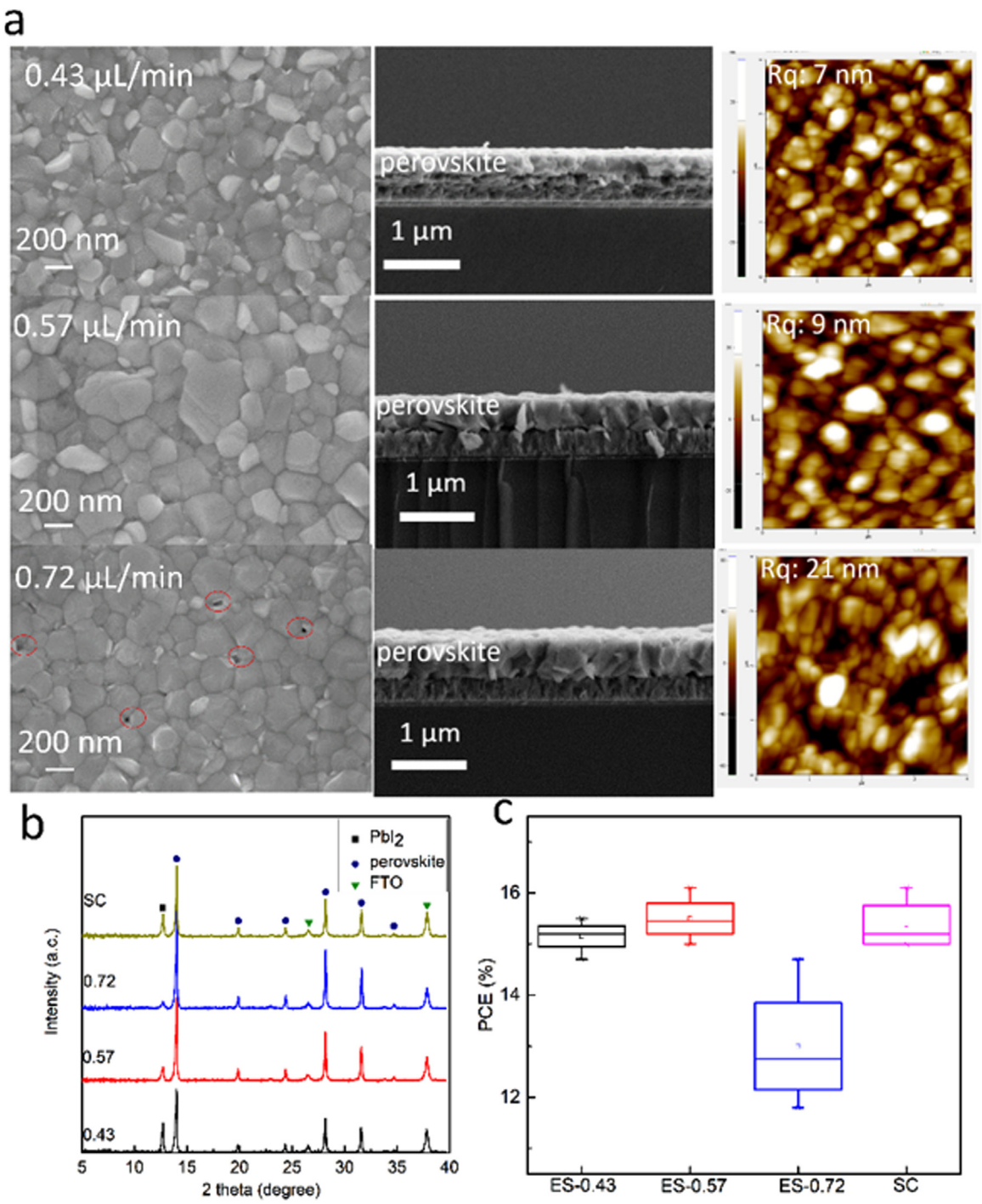

Fig. 3. (a) Top-view, corresponding cross-section view of SEM images and AFM surface scanning images of perovskite films electrospray printed at flow rate of 0.43, 0.57, 0.72 µL/min. (b) XRD and (c) PCE of the devices using electrospray printed and spin-coated perovskite.

forming pin-hole free perovskite films using vacuum flash drying. As shown in the cross-section view SEM images (Fig. 3a), the thickness of films printed at the flow rate of 0.43, 0.57 and 0.72 µL/min are 300, 400 and 500 nm respectively, which is consistent with the values calculated using Eq. (4). The top-view SEM images show that the average perovskite grain size increases with flow rate. At low flow rate (0.43 µL/min), the vacuum flash drying of the thin wet film is completed within seconds, achieving a high degree of supersaturation, which can promote homogeneous and fast crystal nucleation [28]. However, the crystal size is small because of the short time for crystal growth and the small film thickness. When the flow rate is increased to 0.57 µL/min, the longer drying process allows more time for crystal growth which induces larger crystal domains. However, when the flow rate is further increased to 0.72 µL/min, the dried film becomes rougher with pin-holes, which is likely due to the further slowed drying that decreases the degree of supersaturation so that heterogeneous nucleation or secondary nucleation emerges [28]. The root mean square roughness (Rq) of the perovskite films printed at the flow rate of 0.43, 0.57, and 0.72 µL/min are 7 nm, 9 nm, and 21 nm respectively, as indicated by the AFM images in Fig. 3a, in accord with the morphology revealed by SEM images.

The crystalline structure of the electrospray printed perovskite is

examined by the X-ray diffraction (XRD). The XRD spectra of electrospray printed film showed the typical black phase of $FA_{0.85}MA_{0.15}PbI_{2.85}Br_{0.15}$ perovskite diffraction [29], which is the same with that of spin-coated samples (Fig. 3b), indicating that excellent crystalline perovskite can be formed through the electrospray process.

To demonstrate the photovoltaic performance of the electrospray printed perovskite layer, we compared the PCE of the electrospray printed cell and spin-coated cell, as shown in Fig. 3c. The ETL and HTL in the electrospray printed devices were still fabricated by spin-coating. The corresponding J-V curves are shown in Fig. S3. The highest PCE (champion cell: PCE 15.9%) for the device using the electrospray printed perovskite layer at the flow rate of 0.57 μL/min was very close to that of spin-coated PSC (champion cell: PCE 16.1%). This is attributed to the large grain size and smooth surface of perovskite films printed at 0.57 μL/min. Notably, the electrospray printing uses significantly less ink than spin-coating because of high material utilization rate. For example, only 1 μL precursor solution is needed to print a 500 nm thick perovskite film with an area of 20 mm × 15 mm, while at least 20 μL solution is required to coat the same area for spin-coating.

2.3. Electrospray printing of electron transport layer and hole transport layer

The same principle of keeping $t_f < t_e$ is also applied in the electrospray printing of TiO_2 based ETL and Spiro-OMeTAD based HTL. For ETL, the choice of solvent is limited because the TiO_2 nanoparticles were pre-dispersed in deionized water and the addition of other solvent destabilizes the TiO_2 nanoparticles suspension. $t_f < t_e$ can still be guaranteed by reducing t_f through adjusting the working distance. The printed TiO_2 films became smoother as t_f is shortened (Fig. 4a–d). With the shortest t_f, the electrospray printed TiO_2 layer is nearly as smooth as the spin-coated TiO_2. This again confirms the importance of forming wet films for obtaining smooth dry films in electrospray printing process. The *J-V* curves (Fig. 4e) of the spin-coated and electrospray printed FTO/TiO_2/Au structure are virtually indistinguishable, indicating similar conductivity for electrospray printed and spin-coated TiO_2. The PCE data of devices fabricated using spin-coated and electrosprayed TiO_2 films as ETL are shown in Fig. 4f (see *J-V* curve in Fig. S4). Here, perovskite films were electrospray printed and Spiro-OMeTAD were spin-coated for all devices. Not surprisingly, the PCE increases as the TiO_2 film becomes smoother.

For the HTL, in formulating the Spiro-OMeTAD solution, we chose 1,2-dichlorobenzene (DCB) instead of chlorobenzene (CB) as solvent, because DCB has much lower vapor pressure (1.36 mm Hg at 25 °C) than that of CB (12 mm Hg at 25 °C). Thus DCB droplet provides longer evaporation time to ensure wet deposition. Indeed, Spiro-OMeTAD particles were present in the electrospray printed Spiro-OMeTAD film using CB solution due to rapid evaporation, but when CB was replaced by DCB, the electrospray printed Spiro-OMeTAD film is smooth and indistinguishable from that of the spin-coated Spiro-OMeTAD films (inset of Fig. 5). Fig. 5 shows the PCE data of four groups of devices with Spiro-OMeTAD processed under four conditions: (i) spin-coated Spiro-OMeTAD dissolved in CB (SC-CB), (ii) spin-coated Spiro-OMeTAD dissolved in DCB (SC-DCB), (iii) electrospray printed Spiro-OMeTAD dissolved in CB (ES-CB), (iv) electrospray printed Spiro-OMeTAD dissolved in DCB (ES-DCB). Here, both the ETL (TiO_2) and perovskite layer

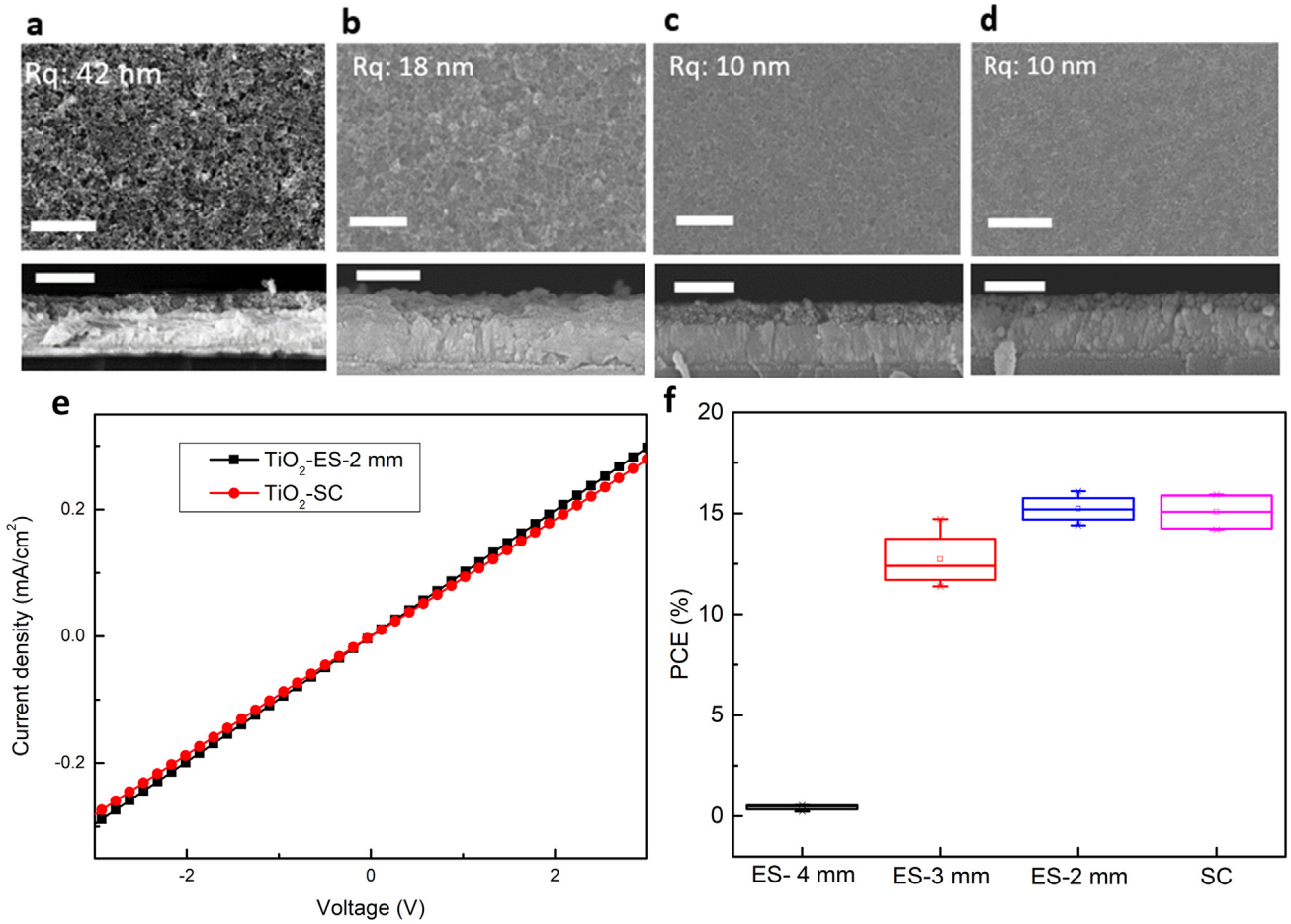

Fig. 4. Top-view and corresponding cross-sectional SEM images of TiO_2 films electrospray printed at working distance of 4 (a), 3 (b), 2 (c) mm and spin-coated (d); The scale bar is 600 nm. (e) Conductivity comparison between the spin-coated TiO_2 film and electrospray printed at 2 mm. (f) PCE of the device using electrospray printed and spin-coated perovskite films.

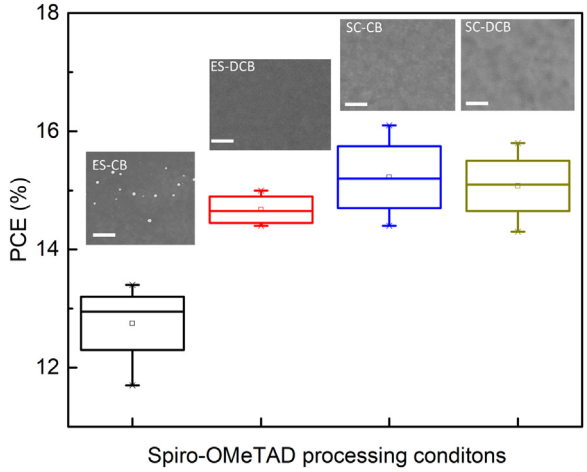

Fig. 5. PCE of PSCs using four different fabrication conditions for Spiro-OMeTAD: electrospray printing with CB or DCB as solvent, and spin-coating with CB or DCB as solvent. The inset shows the corresponding top-view SEM images. The scale bar is 400 nm.

were electrospray printed using the optimal parameters established earlier. The PCEs of the devices using spin-coated Spiro-OMeTAD with CB or DCB as solvent are similar, but for the electrospray printed Spiro-OMeTAD, the PCE is improved from 13.0% (ES-CB) to 15.0% (ES-DCB) (see Fig. S5 for *J-V* curves), suggesting that the improved surface morphology of the printed Spiro-OMeTAD boosts the PCE of devices.

2.4. The performance of all electrospray printed PSC

Finally, we printed all the three functional layers (ETL, perovskite, and HTL) using electrospray process based on the PSC architecture of FTO/TiO_2/$FA_{0.85}MA_{0.15}PbI_{2.85}Br_{0.15}$/Spiro-OMeTAD/Au. The cross-sectional view SEM image (Fig. 6a) of the complete device showed all the three layers are homogeneous and dense. Fig. 6b shows the *J-V* curves of the top performers of the all-printed device, the all spin-coated device, and the device with only perovskite layer was electrospray printed. The photovoltaic metrics of these devices are summarized in Table 1. The all electrospray printed device showed an open-circuit voltage (V_{OC}) of 1.06 V, a short-circuit current (J_{SC}) of 21.9 mA/cm^2, a fill factor (FF) of 64.1% and PCE of 15.0%, which reflect only a modest performance drop from the all-spun devices. The electrospray printed perovskite based device showed higher J_{SC} than the spin-coated perovskite based device, which is owning to the perovskite grains by electrospray printing are larger and more uniform than that from spin-coating (Fig. S2). To examine the reproducibility of the all-printed device, we have conducted *J-V* measurements on one batch of devices and the inset of Fig. 6b shows the PCE distribution, with an average efficiency of 13.6%. The stability of the all-printed devices without encapsulation was also studied. The data (Fig. S6) show that the all electrospray printed devices is fairly stable with only 8% efficiency loss after being stored for 30 days in ambient condition with a relative humidity of ~ 20% at room temperature.

Table 1
Photovoltaic metrics of the all electrospray printed, all spin-coated devices and the device with only the perovskite layer electrospray printed.

Process	V_{oc} (V)	J_{sc} (mA/cm^2)	Fill factor (%)	Champion efficiency (%)	Average efficiency (%)
All electrospray printing	1.06	21.9	64.1	15.0	13.6
All spin-coating	1.10	20.7	70.6	16.1	15.0
Perovskite layer printed by electrospray	1.09	25.0	58.2	15.9	14.7

Prior investigations [11,12,30,31] have shown great promise in the scalable fabrication of high-quality perovskite photoactive layer, enabling PCE up to 20% for PSCs with printed photoactive layer, yet only a limited number of studies have applied the scalable deposition process for all three layers (ETL, perovskite, and HTL) [7,8,32,33]. Especially for those reporting high PCEs, spin-coated [30] or thermal evaporated [11,12] charge transport layers are still required. To the best of our knowledge, the PCE of our all electrospray printed champion cell is the highest for PSCs with all three functional layers fabricated using scalable method in air and at moderate temperature (up to 150 °C), as shown in Table 2. Zheng et al. reported a blow-drying method to fabricate mesoporous TiO_2, methylammonium lead halide ($CH_3NH_3PbI_3$) perovskite and Spiro-OMeTAD layers [15], however, the processing conditions are more demanding, such as N_2 environment and high-temperature annealing (450 °C) for the TiO_2 layer. Recently Zuo et al. [8] demonstrated one-step roll-to-roll air processed perovskite solar cells on a flexible substrate achieving a respectable PCE of 11.16%. They also fabricated devices on glass substrate with only the perovskite slot die coated, and the corresponding PCE is 15.57%, which is comparable with the 15.9% PCE of the device with only perovskite layer printed by electrospray in this work (Table 1).

It is insightful to compare the electrospray printing process to doctor blading, which is highly successful in making micrometer-sized perovskite crystals and reaching one of the highest PCEs to date for PSCs. Electrospray printing generates polycrystalline film with

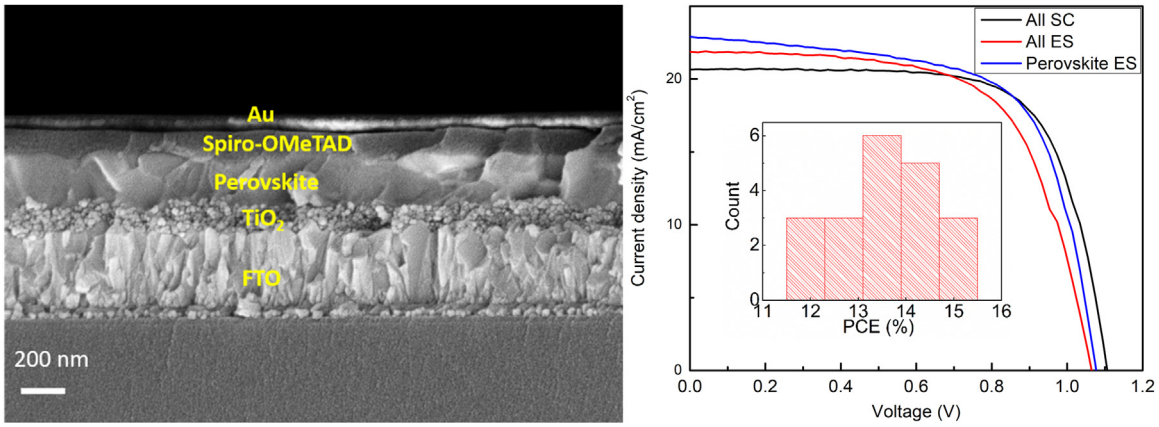

Fig. 6. (a) Cross-section view SEM image of an all electrospray printed PSC. (b) *J-V* curves for the champion cell of the all printed, all spin-coated devices and the device with only perovskite layer electrospray printed. Inset: the PCE distribution histogram of the all printed devices.

Table 2
Overview of PCE of the reported PSCs with all three layers (ETL, perovskite, and HTL) fabricated using scalable methods.

Scalable method	Special conditions[a]	Best PCE	Reference
Infiltration	/	12.8%	[34]
Brush printing	/	9.1%	[35]
Slot-die	/	12.6%	[36]
Doctor blade	Humidity controlled (15–25%)	10.7%	[32]
Slot-die	/	12.0%	[7]
Slot-die	/	14.7%	[33]
Screen-printing	High-temperature (500 °C)	13.3%	[37]
Blow drying	High-temperature (450 °C), glove box	17%	[15]
Electrospray printing	/	15.0%	This work

[a] The special conditions needed including humidity control, environment control and temperature. The omission of a certain condition means this condition is not required during the preparation of PSCs.

characteristic grain size of only ~ 300 nm, which is much smaller than the state-of-art of doctor blading [11]. Interestingly, more than two orders of magnitude increase in grain boundary density did not dramatically deteriorate the PCE (15.0% for all-electrospray printed, 15.9% for perovskite layer electrospray printed only vs 20% for best reported doctor blading data), signifying one important and desirable trait of perovskite, which is the strong defect tolerance [38].

In terms of printing speed, doctor blading has an optimal substrate moving speed of ~ 10 μm/s in the most commonly operated evaporation region. Recently the speed of ~ 50 mm/s has been reached in the Landau-Levich region by adding surfactant to suppress surface flow instability [12]. The printing speed for the electrospray is ~ 10 mm/s, which is much faster than the doctor blading operated in the evaporating region and comparable with that in the Landau-Levich region. The throughput of electrospray printing can be dramatically scaled-up because large arrays of 91–331 emitters have been demonstrated [39]. Furthermore, the electrospray printing may complement the doctor blading when the substrate has relatively high surface roughness or is non-flat along the direction that is perpendicular to the substrate moving direction.

3. Conclusion

We have succeeded in fabricating efficient PSCs devices using electrospray to print all three layers (ETL, perovskite, and HTL) in air and below 150 °C. Choosing short working distances and solvents with low vapor pressure such as GBL, NMP and DCB ensures that the droplet evaporation time is longer than the droplet flying time, which enables wet film deposition. Such electrospray printing process results in pinhole free, homogeneous and smooth perovskite films. The results demonstrate that electrospray is able to print uniform functional films from sub-100–500 nm range, making it a powerful tool to coat or pattern functional layers of perovskite optoelectronic devices. The PCE of the all printed devices reached up to 15.0%. Our results demonstrate that the electrospray printed PSCs can provide performance on par with spin-coated cells in terms of active layer morphology and overall device performance. In addition, electrospray printing offers benefits of roll-to-roll compatibility and nearly zero material waste. More importantly, electrospray can be massively multiplexed [40], providing a feasible route for large-scale manufacturing of PSCs and paving the way for roll-to-roll printing on flexible substrates.

4. Experimental section

4.1. Solution preparation and device fabrication

$CH_3(NH)_2I$, CH_3NH_3Br powders and PbI_2 were added in a mixture of γ-Butyrolactone (GBL) and1-Methyl-2-pyrrolidinone (NMP) (7:3 v/v) to make 1 M $FA_{0.85}MA_{0.15}PbI_{2.85}Br_{0.15}$ solution. All chemicals are purchased from Sigma-Aldrich and used as received without further purification. Mix Ti-Nanoxide T-L paste (Solaronix) with DI water and tert-butyl alcohol, followed by stirring for 2 h and ultrasonic dispersing for 30 min. Dissolve 36 mg of Spiro-OMeTAD in 1 mL 1,2-Dichlorobenzene, with addition of 23 μL Li-TFSI/acetonitrile (170 mg/mL), 75 μL of [tris (2-(1H-pyr- azol-1-yl)-4-tert-butylpyridine) cobalt (III) bis (trifluoromethylsulphonyl) imide] (FK209) /acetonitrile (100 mg/mL) and 10 μL of 4-tert-butylpyridine (TBP). Before electrospray printing, the Spiro-OMeTAD solution was diluted to 7.2 mg/mL. The glass/FTO substrate was successively washed with Hellmanex III, acetone, ethanol and DI water. The sheet resistance of FTO is 12–14 Ω/sq and the thicknesses of glass and FTO are 2.2 mm and 200 nm, respectively. The average transmittance of glass/FTO in the visible region is around 82–84.5%. The electrospray printing process took place in a fume hood in ambient atmosphere. Fig. 1a illustrates the electrospray printing apparatus, which consists of an electrospray emitter on a syringe driven by a syringe pump, a high voltage DC power supply, a cone-jet visualization subsystem, and a substrate motion control subsystem. Prior to printing, the prepared solution was loaded into a syringe and the flow rate was controlled by the syringe pump. The substrate and the syringe were mounted on a computer controlled motorized linear stage and a serpentine path motion of electrospray nozzle relative to substrate as shown in Fig. 1e was designed. TiO_2, perovskite and Spiro-OMeTAD film were printed sequentially on the pre-cleaned FTO glass. Table S1 summarizes the parameters such as working distance, flow rate and printing speed for printing TiO_2, perovskite and Spiro-OMeTAD. The TiO_2 layer was printed first, and the sample was annealed at 150 °C for 30 min. The perovskite film was printed on the annealed TiO_2 layer, and after the wet perovskite precursor film was printed, the sample underwent flash vacuum drying in a vacuum chamber which induces rapid sample drying within a few seconds. The sample with dry perovskite film was annealed on a hotplate at 150 °C for 15 min. Next, the Spiro-OMeTAD layer was printed on top of the perovskite film. Similarly, the sample with wet Spiro-OMeTAD was dried by flash vacuum. Finally, an 80 nm thick gold layer was evaporated as the top electrode. The active area of each device was 0.1 cm^2.

4.2. Characterization

X-ray diffraction (XRD) analyses were performed at a scanning rate of 5°/min on an X-ray diffractometer (Philips Xpert Pro). Scanning electron microscopy images were obtained from scanning electron microscope (Zeiss 1550) operated at an accelerating voltage of 5 kV. Photovoltaic performance of the solar cells was analyzed under one sun (AM 1.5 G, 100 mW/cm^2) illumination with a solar simulator (150 W Sol 2ATM, Oriel), and the current-voltage characteristics of each cell were recorded with a digital source meter (Keithley 2400). AFM images were obtained from atomic force microscope (Parker XE7) in the dark.

Acknowledgements

W.D. gratefully acknowledges the funding support from National Science Foundation, United States (CMMI 1301099 and CMMI 1549917). S.P. acknowledges the support from Centers of Research Excellence in Science and Technology, National Science Foundation, United States (HRD 1547771). C.W. acknowledge the funding support from the SBIR program through Nanosonic, United States. J.C. and W.C. acknowledge the funding support from National Natural Science Foundation of China (NSFC 51328601), National Science Foundation, United States (NSF ECCS 1550749) and Virginia Tech ICTAS Junior Faculty Award. X.Z. and Z.T. acknowledge the funding support from National Natural Science Foundation of China (NSFC 61605076), K.W. acknowledges the support from Office of Naval Research, United States (N000141613043).

Conflict of interest

The authors declare no conflict of interest

Appendix A. Supporting information

Supplementary data associated with this article can be found in the online version at doi:10.1016/j.nanoen.2018.08.062.

References

[1] M.A. Green, A. Ho-Baillie, H.J. Snaith, The emergence of perovskite solar cells, Nat. Photonics 8 (2014) 506–514, https://doi.org/10.1038/nphoton.2014.134.

[2] J. Huang, Y. Shao, Q. Dong, Organometal trihalide perovskite single crystals: a next wave of materials for 25% efficiency photovoltaics and applications beyond? J. Phys. Chem. Lett. 6 (2015) 3218–3227, https://doi.org/10.1021/acs.jpclett.5b01419.

[3] A. Kojima, K. Teshima, Y. Shirai, T. Miyasaka, Organometal halide perovskites as visible-light sensitizers for photovoltaic cells, J. Am. Chem. Soc. 131 (2009) 6050–6051, https://doi.org/10.1021/ja809598r.

[4] M.M. Lee, J. Teuscher, T. Miyasaka, T.N. Murakami, H.J. Snaith, Efficient hybrid solar cells based on meso-superstructured organometal halide perovskites, Science 338 (2012) 643–647, https://doi.org/10.1126/science.1228604.

[5] J. Burschka, N. Pellet, S.J. Moon, R. Humphry-Baker, P. Gao, M.K. Nazeeruddin, M. Grätzel, Sequential deposition as a route to high-performance perovskite-sensitized solar cells, Nature 499 (2013) 316–319, https://doi.org/10.1038/nature12340.

[6] NREL. Efficiency chart. https://www.nrel.gov/pv/assets/images/efficiency-chart-20180716.jpg, 2018.

[7] K. Hwang, Y.S. Jung, Y.J. Heo, F.H. Scholes, S.E. Watkins, J. Subbiah, D.J. Jones, D.Y. Kim, D. Vak, Toward large scale roll-to-roll production of fully printed perovskite solar cells, Adv. Mater. 27 (2015) 1241–1247, https://doi.org/10.1002/adma.201404598.

[8] C. Zuo, D. Vak, D. Angmo, L. Ding, M. Gao, One-step roll-to-roll air processed high efficiency perovskite solar cells, Nano Energy 46 (2018) 185–192, https://doi.org/10.1016/j.nanoen.2018.01.037.

[9] Y. Deng, E. Peng, Y. Shao, Z. Xiao, Q. Dong, J. Huang, Scalable fabrication of efficient organolead trihalide perovskite solar cells with doctor-bladed, Energy Environ. Sci. 8 (2015) 1544–1550, https://doi.org/10.1039/C4EE03907F.

[10] Y. Deng, Q. Dong, C. Bi, Y. Yuan, J. Huang, Air-stable, efficient mixed-cation perovskite solar cells with Cu electrode by scalable fabrication of active layer, Adv. Energy Mater. 6 (2016) 1–6, https://doi.org/10.1002/aenm.201600372.

[11] W. Wu, Q. Wang, Y. Fang, Y. Shao, S. Tang, Y. Deng, H. Lu, Y. Liu, T. Li, Z. Yang, A. Gruverman, J. Huang, Molecular doping enabled scalable blading of efficient hole-transport-layer-free perovskite solar cells, Nat. Commun. 9 (2018) 1625, https://doi.org/10.1038/s41467-018-04028-8.

[12] Y. Deng, X. Zheng, Y. Bai, Q. Wang, J. Zhao, J. Huang, Surfactant-controlled ink drying enables high-speed deposition of perovskite films for efficient photovoltaic modules, Nat. Energy 3 (2018) 560–566, https://doi.org/10.1038/s41560-018-0153-9.

[13] Z. Wei, H. Chen, K. Yan, S. Yang, Inkjet printing and instant chemical transformation of a $CH_3NH_3PbI_3$/nanocarbon electrode and interface for planar perovskite solar cells, Angew. Chem. - Int. Ed. 53 (2014) 13239–13243, https://doi.org/10.1002/anie.201408638.

[14] A. Barrows, A. Pearson, C. Kwak, A. Dunbar, A. Buckley, D. Lidzey, Efficient planar heterojunction mixed-halide perovskite solar cells deposited via spray-deposition, Energy Environ. Sci. 7 (2014) 1–7, https://doi.org/10.1039/C4EE01546K.

[15] J. Zheng, M. Zhang, C.F.J. Lau, X. Deng, J. Kim, Q. Ma, C. Chen, M.A. Green, S. Huang, A.W.Y. Ho-Baillie, Spin-coating free fabrication for highly efficient perovskite solar cells, Sol. Energy Mater. Sol. Cells 168 (2017) 165–171, https://doi.org/10.1016/j.solmat.2017.04.029.

[16] M. Cloupeau, B. Prunet-Foch, Electrostatic spraying of liquids in cone-jet mode, J. Electrost. 22 (1989) 135–159, https://doi.org/10.1016/0304-3886(89)90081-8.

[17] W. Deng, A. Gomez, The role of electric charge in microdroplets impacting on conducting surfaces, Phys. Fluids 22 (2010) 1–4, https://doi.org/10.1063/1.3431739.

[18] P.-Y. Lin, Y.-Y. Chen, T.-F. Guo, Y.-S. Fu, L.-C. Lai, C.-K. Lee, Electrospray technique in fabricating perovskite-based hybrid solar cells under ambient conditions, RSC Adv. 7 (2017) 10985–10991, https://doi.org/10.1039/C6RA27704G.

[19] S.C. Hong, G. Lee, K. Ha, J. Yoon, N. Ahn, W. Cho, M. Park, M. Choi, Precise morphology control and continuous fabrication of perovskite solar cells using droplet-controllable electrospray coating system, ACS Appl. Mater. Interfaces 9 (2017) 7879–7884, https://doi.org/10.1021/acsami.6b15095.

[20] S. Kavadiya, D.M. Niedzwiedzki, S. Huang, P. Biswas, Electrospray-assisted fabrication of moisture-resistant and highly stable perovskite solar cells at ambient conditions, Adv. Energy Mater. 7 (2017) 1–9, https://doi.org/10.1002/aenm.201700210.

[21] J. Fernández de la Mora, The fluid dynamics of taylor cones, Annu. Rev. Fluid Mech. 39 (2007) 217–243, https://doi.org/10.1146/annurev.fluid.39.050905.110159.

[22] Y. Wei, W. Deng, R.H. Chen, Effects of insoluble nano-particles on nanofluid droplet evaporation, Int, J. Heat Mass Transf. 97 (2016) 725–734, https://doi.org/10.1016/j.ijheatmasstransfer.2016.02.052.

[23] E.J. Juarez-Perez, R.S. Sanchez, L. Badia, G. Garcia-Belmonte, Y.S. Kang, I. Mora-Sero, J. Bisquert, Photoinduced giant dielectric constant in lead halide perovskite solar cells, J. Phys. Chem. Lett. 5 (2014) 2390–2394, https://doi.org/10.1021/jz5011169.

[24] B. Abramzon, W.A. Sirignano, Droplet vaporisation model for spray combustion calculations, Int. J. Heat Mass Transf. 9 (1989) 1605–1618.

[25] S. Kavadiya, R. Raliya, M. Schrock, P. Biswas, Crumpling of graphene oxide through evaporative confinement in nanodroplets produced by electrohydrodynamic aerosolization, J. Nanopart. Res. 19 (2017) 43, https://doi.org/10.1007/s11051-017-3738-5.

[26] C.V. Sternling, L.E. Scriven, Interfacial turbulence: hydrodynamic instability and the marangoni effect, AIChE J. 5 (1959) 514–523, https://doi.org/10.1002/aic.690050421.

[27] X. Li, D. Bi, C. Yi, J.-D. Decoppet, J. Luo, S.M. Zakeeruddin, A. Hagfeldt, M. Gratzel, A vacuum flash-assisted solution process for high-efficiency large-area perovskite solar cells, Science 353 (2016) 58–62, https://doi.org/10.1126/science.aaf8060.

[28] Y. Yu, S. Yang, L. Lei, Y. Liu, Nucleation mediated interfacial precipitation for architectural perovskite films with enhanced photovoltaic performance, Nanoscale 9 (2017) 2569–2578, https://doi.org/10.1039/C6NR08741H.

[29] N.J. Jeon, J.H. Noh, W.S. Yang, Y.C. Kim, S. Ryu, J. Seo, S. Il Seok, Compositional engineering of perovskite materials for high-performance solar cells, Nature 517 (2015) 476–480, https://doi.org/10.1038/nature14133.

[30] M. He, B. Li, X. Cui, B. Jiang, Y. He, Y. Chen, D. O'Neil, P. Szymanski, M.A. EI-Sayed, J. Huang, Z. Lin, Meniscus-assisted solution printing of large-grained perovskite films for high-efficiency solar cells, Nat. Commun. 8 (2017) 16045, https://doi.org/10.1038/ncomms16045.

[31] J. Li, R. Munir, Y. Fan, T. Niu, Y. Liu, Y. Zhong, Z. Yang, Y. Tian, B. Liu, J. Sun, D.M. Smilgies, S. Thoroddsen, A. Amassian, K. Zhao, S. (Frank) Liu, Phase transition control for high-performance blade-coated perovskite solar cells, Joule 2 (2018) 1–18, https://doi.org/10.1016/j.joule.2018.04.011.

[32] Z. Yang, C.C. Chueh, F. Zuo, J.H. Kim, P.W. Liang, A.K.Y. Jen, High-performance fully printable perovskite solar cells via blade-coating technique under the ambient condition, Adv. Energy Mater. 5 (2015) 1–6, https://doi.org/10.1002/aenm.201500328.

[33] T. Qin, W. Huang, J.E. Kim, D. Vak, C. Forsyth, C.R. McNeill, Y.B. Cheng, Amorphous hole-transporting layer in slot-die coated perovskite solar cells, Nano Energy 31 (2017) 210–217, https://doi.org/10.1016/j.nanoen.2016.11.022.

[34] A. Mei, X. Li, L. Liu, Z. Ku, T. Liu, Y. Rong, M. Xu, M. Hu, J. Chen, Y. Yang, M. Grätzel, H. Han, A hole-conductor-free, fully printable mesoscopic perovskite solar cell with high stability, Science 345 (2014) 295–298, https://doi.org/10.1126/science.1254763.

[35] J.-W. Lee, S.-I. Na, S.-S. Kim, Efficient spin-coating-free planar heterojunction perovskite solar cells fabricated with successive brush-painting, J. Power Sources 339 (2017) 33–40, https://doi.org/10.1016/j.jpowsour.2016.11.028.

[36] Y.-S. Jung, K. Hwang, Y.-J. Heo, J.-E. Kim, D. Lee, C.-H. Lee, H.-I. Joh, J.-S. Yeo, D.-Y. Kim, One-step printable perovskite films fabricated under ambient conditions for efficient and reproducible solar cells, ACS Appl. Mater. Interfaces 9 (2017) 27832–27838, https://doi.org/10.1021/acsami.7b05078.

[37] A. Bashir, S. Shukla, J.H. Lew, S. Shukla, A. Bruno, D. Gupta, T. Baikie, R. Patidar, Z. Akhter, A. Priyadarshi, N. Mathews, S.G. Mhaisalkar, Spinel Co_3O_4 nanomaterials for efficient and stable large area carbon-based printed perovskite solar cells, Nanoscale 10 (2018) 2341–2350, https://doi.org/10.1039/C7NR08289D.

[38] M.V. Kovalenko, L. Protesescu, M.I. Bodnarchuk, Properties and potential optoelectronic applications of lead halide perovskite nanocrystals, Science 750 (2017) 745–750, https://doi.org/10.1126/science.aam7093.

[39] W. Deng, C.M. Waits, B. Morgan, A. Gomez, Compact multiplexing of monodisperse electrosprays, J. Aerosol Sci. 40 (2009) 907–918, https://doi.org/10.1016/j.jaerosci.2009.07.002.

[40] W. Deng, J.F. Klemic, X. Li, M.A. Reed, A. Gomez, Increase of electrospray throughput using multiplexed microfabricated sources for the scalable generation of monodisperse droplets, J. Aerosol Sci. 37 (2006) 696–714, https://doi.org/10.1016/j.jaerosci.2005.05.011.

Yuanyuan Jiang is currently pursuing a Ph.D. degree in Mechanical Engineering at Virginia Tech. She received her B.E. degree in Material chemistry in 2012 from central South University and her master degree in Materials Science in 2015 from Chinese Academy of Sciences. Her research focuses on electrospray printing and perovskite solar cells.

Congcong Wu is currently a Research Associate in the Center for Energy Harvesting Materials and Systems at Virginia Tech. He received his B.S. degree in Material Science in 2007, and Ph.D. degree in Material Science in 2014 from Huazhong University of Science and Technology. His research focuses on nanomaterial synthesis, interfacial charge transfer kinetics, and dye-sensitized/perovskite solar cells.

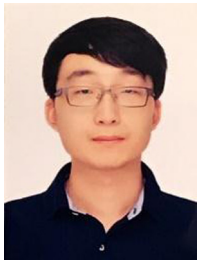

Liurui Li is currently a Ph.D. candidate in the Energy Storage System Lab at Virginia Tech. He received his B.S. degree in Mechanical Engineering in 2016 from Shandong University, and M.S. degree in Mechanical Engineering in 2017 from Virginia Tech. His research focused on silicone based multiplexed electrospray system and battery recycling system design.

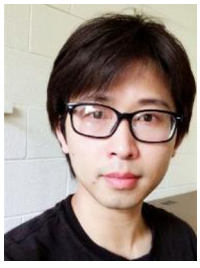

Kai Wang obtained his Ph.D. degree in Polymer Engineering in 2017 from The University of Akron and joined the Center for Energy Harvesting Materials and System (CEHMS) at Virginia Tech as a Postdoctoral Associate at the same year. His research interests include halide perovskite photovoltaics, two-dimensional multiple quantum well physics and bioelectronics.

Zui Tao is currently working at Visionox Tech Inc. as a CVD Process Researcher. He received his B.E. degree in Photoelectric Materials and Devices in 2015 and master degree in Materials Science in 2018 from Nanjing Tech University. During his post-graduate period, his research focused on electrospray preparing organic perovskite solar cells.

Fan Gao is currently a Ph.D. student in Mechanical Engineering Department at Virginia Tech. He received his B.S. degree in Mechatronics Engineering in 2014 from Zhejiang University. His research focuses on droplet, lubrication theory and electrohydrodynamics.

Weifeng Cheng is currently a 3rd year Ph.D. student in Mechanical Engineering department at Virginia Tech. He received his B.S. degree in Thermal Energy and Power Engineering in 2013 from Jilin University, and he earned his M.S. degree in Mechanical Engineering in 2014 from UC Berkeley. His research area is concentrated on electrowetting on dielectric (EWOD), microfluidics, and surface wettability.

Dr. Jiangtao Cheng received his Ph.D. degree in Physics from *Purdue University* in 2002. He also has a M.S. degree in Computer Science from *Purdue University* and a B.S. degree in Applied Physics from *Peking University* at Beijing. Prior to joining the Department of Mechanical Engineering at *Virginia Tech* in 2015 as Associate Professor, Dr. Cheng was a research associate at *the Pennsylvania State University* and a research scientist at *Teledyne Scientific Company* (formerly *Rockwell Science Center*). He has extensive experience in optofluidics, thermal-fluid sciences, renewable energy, micro/nano-fluidics, multiphase fluid flow, nano-fabrications and CFD numerical simulation.

Dr. Xin-Yan Zhao received her B.S. degree from Xi'an Technological University, China, in 1999; the M.S. degree from Beijing Institute of Technology, China, in 2003; and Ph.D. degree from Nanjing University of Posts and Telecommunications, China, in 2014. She is currently a research assistant professor at the Southern University of Science and Technology, China. Her research areas include mechanism of optoelectronic devices, nanostructure and characteristics of optoelectronic devices, fabrication of flexible organic thin-films by electrospray, flexible and stretchable electrodes and applications in optoelectronic devices.

Dr. Shashank Priya is currently Professor in department of materials science and engineering at Penn State and adjunct Professor in department of mechanical engineering at Virginia Tech. At Penn State, he is also serving as associate vice-president for research and director of strategic initiatives. His research is focused in the areas related to multifunctional materials, energy and bio-inspired systems. He has published over 350 peer-reviewed journal papers and more than 60 conference proceedings covering these topics. Additionally, he has published more than seven US patents, and ten edited books. He is currently serving as founding president of the "Energy Harvesting Society", editorial board member of journal integrated ferroelectrics and Honorary Chair Committee member for the International Workshop on Piezoelectric Materials and Applications (IWPMA). Shashank has received several awards including: Alumni award for excellence in Research 2014, Fellow American Ceramic Society 2013, Turner Fellowship 2012, Dean's Research Excellence Award 2011, and AFOSR Young Investigator Award.

Dr. Weiwei Deng is a Professor in the Department of Mechanics and Aerospace Engineering at the Southern University of Science and Technology (SUSTech). Before joining SUSTech in 2017, he was a tenured Associate Professor at Virginia Tech. Dr. Deng received his Ph.D. from Yale University in 2008 and M.S./B.S. from Tsinghua University in 2001. His research interest is the experimental fluid dynamics of droplets, jets, and thin films. He is also interested in processing advanced functional materials through printing of liquid droplets. Dr. Deng received the National Science Foundation CAREER Award in 2015.